The *p*H of CO_2–saturated aqueous KCl solutions at temperatures between 298 K and 423 K at pressures up to 13.5 MPa

Meiheriayi Mutailipu,[a,b,c] Yu Liu,[b] Yongchen Song,[b] and J P Martin Trusler[a,*]

[a] Department of Chemical Engineering, Imperial College London, South Kensington Campus, London SW7 2AZ, United Kingdom

[b] Key Laboratory of Ocean Energy Utilization and Energy Conservation of the Ministry of Education, Dalian University of Technology, Dalian 116024, China

[c] School of Electrical Engineering, Xinjiang University, Urumqi 830047, China

* Corresponding author, email: m.trusler@imperial.ac.uk

ABSTRACT

The *p*H of CO_2-saturated brines is of importance in geological carbon storage utilizing saline aquifers as it is a key variable controlling fluid-mineral chemical reactions that affect CO_2 storage capacity and security. In this paper, we report experimental measurements of the *p*H of CO_2-saturated aqueous KCl solutions carried out using high-pressure glass and ZrO_2 *p*H electrodes, coupled with a Ag/AgCl reference electrode, at a temperatures from (298 to 423 K) and at pressure between (0.2 and 13.5) MPa. The results are in good agreement with values predicted using the Pitzer model with the McInnes convention as implemented in the PHREEQC geochemical simulator software. The *p*H of CO_2-saturated KCl solutions decreases with increasing partial pressure of CO_2 and increases with increasing temperature. Increasing the molality of the KCl solutions tends to lower the *p*H but not as rapidly as is the case the NaCl.

Keywords: CO_2; Carbon storage; *p*H; Pitzer model; Potassium chloride

1. Introduction

Reducing the emissions of CO_2, the main greenhouse gas, has become one of the most pressing concerns facing modern society. Among the many actions that can contribute to this objective, carbon capture and storage (CCS) remains critically important. Due to their vast potential capacity, deep saline aquifers have been identified as favorable sinks for geological carbon storage (GCS) (Bachu, 2000; Metz, 2005), the final link in the CCS chain . In GCS, injected CO_2 may be retained within a sedimentary basin by a combination of four mechanisms: (1) structural trapping of mobile and buoyant CO_2 below impermeable caprocks; (2) residual trapping of dispersed micro-bubbles of CO_2 by capillary forces within the brine-wetted pore space; (3) solubility trapping in which CO_2 dissolves into the reservoir fluids; and (4) slow chemical reactions with the reservoir rocks leading to mineralization (Bachu, 2000; Metz, 2005). The process of CO_2 dissolution in reservoir brines leads to a lowering of the *p*H and, consequently, to altered chemical interactions with the reservoir rocks and the phenomena of reactive transport (Kaszuba et al., 2003). This may have multiple effects, such as dissolution of reservoir minerals in regions of high dissolved CO_2 concentration and precipitation of minerals elsewhere in the reservoir, possibly leading to undesirable reductions in porosity and permeability. Generally, the *p*H of CO_2-saturated reservoir brines has a strong influence on the reaction rates and the vapor-liquid-solid equilibria of the system, with consequent changes in the seepage, porosity and permeability characteristics of the formation (Druckenmiller and Maroto-Valer, 2005; Morse and Arvidson, 2002). Thus, it is necessary to have a sound understanding of the *p*H of CO_2-saturated brines in order to design a safe and effective GCS project utilizing a saline aquifer and to model processes such as well stimulation, seal leakage and injectivity (Alkhaldi et al., 2010).

According to the International Union of Pure and Applied Chemistry (IUPAC) (Covington et al., 1985), *p*H is defined as $-\log_{10}(\alpha_{H^+}/m^\circ)$ where α_{H^+} is the hydrogen ion activity on a molality scale and $m^\circ = 1\ \mathrm{mol \cdot kg^{-1}}$. However, direct measurement of single-ion activities is not possible and practical realizations of *p*H involve additional assumptions. In general, there are two viable methods for measuring the *p*H of CO_2-saturated brine or water: electrometric and optical techniques. The potential difference or e.m.f of an electrode system immersed in the solution forms the basis of the electrometric method while, in the optical method, *p*H is obtained by measuring the absorption spectrum of an indicator dye. The optical methods, typically based on UV–vis spectrophotometry, have recently been used in determining the *p*H of aqueous solutions and can be considered simple, rapid, and precise. For example, the *p*H of seawater has been measured via the optical method with a very high precision of ±0.004 *p*H units (Byrne and Breland, 1989; Clayton and Byrne, 1993; Robert-Baldo et al., 1985). The setup for the electrometric method involves two electrodes: a *p*H electrode with, for example, either a glass

or a zirconia membrane, and a reference electrode (usually Ag/AgCl). However, this method introduces a liquid junction and associated potential that affects the accuracy of the measured *p*H (Marion et al., 2011). Nevertheless, the availability of commercial *p*H and reference electrodes with high-pressure and high-temperature capabilities, makes the electrometric method well suited to measuring the *p*H of gas-saturated aqueous solutions under high-pressure and/or high-temperature conditions.

Whichever measurement approach is adopted, careful calibration of the measurement system is essential, together with the adoption of a practical convention to replace the formal definition of *p*H. For measurements in aqueous media at low ionic strength (< 0.1 $mol \cdot kg^{-1}$), the Bates-Guggenheim convention (Covington et al., 1985) is the accepted way to realize an operational definition of *p*H. Standard buffer solutions, of accurately known *p*H according to the Bates-Guggenheim convention, are available for calibration. Measurements of the *p*H of CO_2-saturated water fall within this low-ionic-strength regime. However, for the higher ionic strengths typical of reservoir brines, different operational definitions of *p*H are in use and hence measurements may not be unique. In this situation, it is necessary to adopt a well-defined convention and to apply it consistently in both calibration and measurement. In our work, we adopt the MacInnes convention (MacInnes, 1919) whereby the activity coefficients of K^+ and Cl^- are taken to be identical and equal to the mean ionic activity coefficient $\gamma_{\pm}$ for KCl at the same temperature and molality.

Previous work on the *p*H of CO_2-saturated aqueous solutions has focused mainly on water (Meyssami et al., 1992; Parton et al., 2002; Peng et al., 2013; Rosenqvist et al., 2012; Toews et al., 1995), seawater (Kimuro et al., 1994) and NaCl brines (Crolet and Bonis, 1983; Haghi et al., 2017; Hinds et al., 2009; Li et al., 2018; Millero et al., 2009; Schaef et al., 2003; Schaef and McGrail, 2005; Shao et al., 2013; Truche et al., 2016). Table 1 summarizes the available data and the corresponding ranges of ionic strength, temperature and pressure. Reservoir brines contain many other ions apart from Na^+ and Cl^-, including K^+, Ca^{2+}, Mg^{2+}, SO_4^{2-}, HCO_3^- and CO_3^{2-}, and these are expected to influence the fluid properties significantly (Aggelopoulos et al., 2010; Hoballah, 2017; Hyde et al., 2017). Measurements on brines containing salts other than or in addition to NaCl have been carried out by Stefansson et al. (Stefánsson et al., 2013), who studies systems containing Na_2CO_3, $NaHCO_3$, NaOH, HCl and NaCl, and by Li et al. who studied both NaCl and $NaHCO_3$ brines (Li et al., 2018). However, to the best of our knowledge there are no measurements of the *p*H of CO_2 saturated KCl solutions at reservoir conditions available in the literature.

Table 1 Literature review for the *p*H measurement of CO_2-saturated aqueous solutions.

Aqueous phase	*I*/(mol kg^{-1})	Method	*T*/K	*p*/MPa	Source
H_2O	0	EL	305–315	0–35	(Meyssami et al., 1992)
H_2O	0	OPT	298–343	7–20	(Toews et al., 1995)
H_2O	0	OPT	298–343	7–20	(Parton et al., 2002)
H_2O	0	EL	294	0–1	(Rosenqvist et al., 2012)
H_2O	0	EL	308–423	0–15	(Peng et al., 2013)
Seawater	~ 0.6	EL	273–294	10–30	(Kimuro et al., 1994)
NaCl (aq)	0 - 3.5	EL	289–347	0.1	(Crolet and Bonis, 1983)
NaCl (aq)	0 -4.5	EL	295–343	0.1–11	(Schaef et al., 2003; Schaef and McGrail, 2005)
NaCl (aq)	0 -4.3	EL	298	0.1	(Hinds et al., 2009)
NaCl (aq)	0 – 5.5	OPT	278-318	0.1	(Millero et al., 2009)
NaCl (aq)	0 – 3.0	OPT	298–366	0–20	(Shao et al., 2013)
NaCl (aq)	0 -1.4	EL	473–553	0.1–15	(Truche et al., 2016)
NaCl (aq)	0.03 – 5.5	EL, OPT	298–353	0–6	(Haghi et al., 2017)
NaCl (aq), $NaHCO_3$ (aq)	0.01 – 5.0	EL	308–373	0.2–15.3	(Li et al., 2018)
Complex brine	0 – 0.43	OPT	298–473	1–2	(Stefánsson et al., 2013)

EL = Electrometric, OPT = optical.

Modelling the *p*H of gas-saturated aqueous solutions is typically carried out with the aid of geochemical simulators, such as PHREEQC (Parkhurst and Appelo, 2013) and EQ3NR (Wolery, 1983). These implement the Pitzer model for the calculation of the activity coefficients of solutes in the aqueous phase, correlations of Henry's constant and an equation of state for gaseous components, and correlations of the standard equilibrium constants for aqueous-phase chemical reactions. The Pitzer model is applicable to both ionic and molecular species in solution over a broad range of ionic strengths up to as much as 20 mol·kg^{-1} (Pitzer, 1973, 1975; Pitzer, 1991; Pitzer and Mayorga, 1973). Interaction parameters needed for the application of this model and have been reported in the literature for many systems including NaCl, $KHCO_3$, K_2CO_3 and KCl solutions over wide ranges of temperature (Appelo, 2015; Parkhurst and Appelo, 2013; Pitzer, 1975; Pitzer, 1991; Pitzer et al., 1984; Plummer et al., 1988; Ruaya and Seward, 1987; Truche et al., 2016; Wolery, 1983; Zhang et al., 2005). With the adoption of *e.g.* the MacInnes convention, the Pitzer model provides single-ion activity coefficients and can therefore be used to compute the *p*H of aqueous solutions. In previous work on NaCl and $NaHCO_3$ brines, the Pitzer model was found to account well for the measured *p*H over wide ranges of temperature, pressure and ionic strength (Li et al., 2018). This type of model offers a very convenient route to predicting the *p*H of complex brines with dissolved CO_2 but additional validation is needed for brines other than NaCl (aq).

In view of the lack of experimental data, the main objective of the present work was to make measurements of the *p*H of CO_2-saturated KCl (aq) over wide ranges of temperature, pressure and molality. The results of these experiments are compared with calculations based on the Pitzer model. Although K^+ molalities in reservoir brines are usually quite small, high levels of K^+ are found in some high-salinity reservoir brines (Hanor, 1994) and in synthetic solutions used in laboratory core-flooding experiments (Pentland et al., 2011). Furthermore, as an unreactive salt, KCl at low molalities has a correspondingly small influence on *p*H. Therefore, to allow a sensitive comparison with the available models, experimental data at relatively high molality were required and, for that reason, the present study focused on KCl molalities of 2 and 4 $mol \cdot kg^{-1}$.

2. Experimental section

2.1 Apparatus

The *p*H value of CO_2-saturated KCl solutions was measured by the electrometric method. The apparatus is shown in Fig. 1 and has been described in detail in previous publication (Li et al., 2018; Peng et al., 2013).

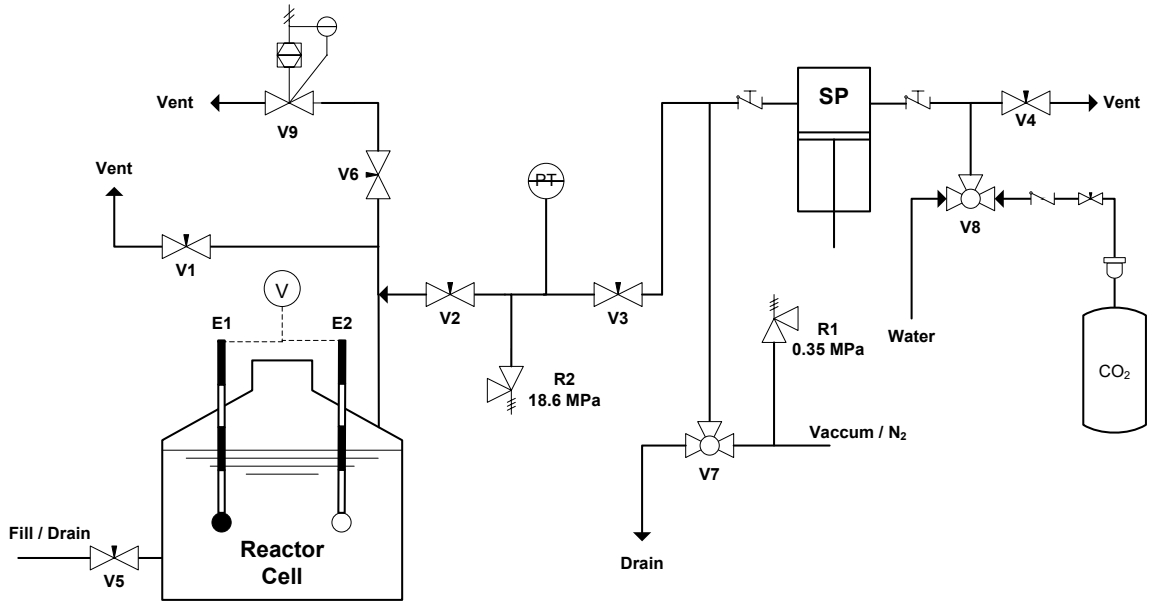

Fig. 1 Schematic of the high-pressure *p*H measurement system for CO_2-saturated aqueous solutions: E1, E2, *p*H measurement and reference electrodes; V, digital voltmeter; SP, syringe pump; R1, R2, pressure relief valves (with relief pressure indicated); PT, pressure transducer; V1 to V6, needle valves; V7, V8, three way ball valves; V9, back-pressure regulator. Reprinted from (Peng et al., 2013), copyright 2013, with permission from Elsevier.

The reactor vessel and other brine-wetted parts were fabricated from corrosion-resistant titanium or Hastelloy C276, while the syringe pump used for CO_2 injection and pressure control was made of stainless steel. The reactor cell accommodating the aqueous solution and *p*H electrodes was made from commercially pure titanium (grade 2) and had an internal diameter of 40 mm, a depth of 60 mm and a capacity of 91cm^3. This vessel was rated for a maximum working pressure of 24 MPa at 298 K, reducing to 17 MPa at 423 K. The reactor was closed by a flat bolted lid and sealed with Viton a O-ring. The lid was fitted with one pressure port, used to admit CO_2 or N_2, and two ports through which the electrodes were inserted and secured by means of NPT threaded unions sealed with PFTE tape. Two radial pressure ports aligned with the bottom of the internal chamber were also provided; one was plugged, and the other was used for injection and discharge of the desired solutions. To achieve uniform composition and accelerate the attainment of equilibrium, an ellipsoidal PTFE-coated magnetic stirrer bar was placed inside the vessel, and the reactor was placed on the top of a magnetic drive.

To regulate the temperature, a close-fitting aluminum heater shell surrounded the vessel, and a jacket of silicon-rubber foam was wrapped around the exterior to minimize heat loss. Four electric cartridge heaters and a PT-100 temperature sensor were inserted into vertical holes bored in the wall of the heater shell; these were used with a PID process controller to control the temperature. A second PT-100 sensor was inserted into a blind vertical hole drilled in the vessel wall (1.6 mm diameter x 30 mm depth) and used to measure the cell temperature. This was connected to a multiplexing data acquisition unit (Agilent, model 34970A) which measured its resistance.

A high-pressure syringe pump (Teledyne ISCO, model 260D) with a maximum operating pressure of 52 MPa was used for CO_2 injection and pressure control. In order to ensure that the CO_2 remained in the liquid phase within the syringe pump, chilled water at a temperature of 283 K was circulated through a jacket surrounding the pump cylinder, over which a foam insulation jacket was fitted. The fluid pressure was measured by means of a pressure transducer (Omegadyne, MMA series) with a full scale range of 24.5 MPa. The voltage output from the pressure transducer was read with the data acquisition unit.

Table 2 Reference and *p*H electrodes used, where T_{min} and T_{max} are the minimum and maximum operating temperatures and p_{max} is the maximum operating pressure.

Electrode	T_{min}/K	T_{max}/K	p_{max}/MPa
Ag/AgCl Reference	273	423	13.6
Glass *p*H	273	353	13.6
ZrO_2 *p*H	363	513	20.6

The reference and *p*H electrodes used in this work are detailed in Table 2, together with their operating temperature and pressure ranges. The ZrO_2 electrode used a Ag/Ag_2O solid electrode enabling use at temperatures down to 363 K. A digital multimeter (Agilent, model 34460A) with an input impedance > 10^{12} Ω was used to measure the e.m.f developed between the *p*H and reference electrodes. The Ag/AgCl reference electrode is susceptible to damage during depressurization as a result of out gassing from the internal electrolyte, which becomes saturated with gas at high pressures. In order to prevent damage, it was necessary to depressurize very slowly and, for that purpose, a programmable back-pressure regulator (Jesco, model BP-2080) was used to control the rate of depressurize to about 0.5 MPa/h. Slow depressurization also helps to avoid decompression damage to the O-ring seal. Nevertheless, this seal was replaced frequently.

During the measurement, the temperature, pressure and electrode e.m.f. were continuously monitored and logged by a control computer.

2.2 Experimental procedure

Prior to introducing a fresh solution, the vessel was flushed with deionized water and, to avoid dilution of the new brine sample, dried by a flow of N_2. Approximately, 80 cm^3 of the aqueous solution was then injected through valve V5 and, with valves V1, V3, and V6 closed and the syringe pump isolated, the solution was degassed using the vacuum pump with stirring for a few minutes; sufficient to remove dissolved air without removing a significant amount of water from the solution. CO_2 was then admitted from the syringe pump. For pressures below about 4.5 MPa (the vapor pressure of CO_2 at the pump pressure), pressure as adjusted manually be slowly admitting CO_2 through valve V3. At higher pressures, V3 remained open and the pressure was regulated by the syringe pump operating in pressure-control mode. Stirring at approximately 50 rpm was continued for at least four hours to ensure equilibrium. The approach to equilibrium could be monitored by observing both the syringe pump volume and the e.m.f. across the electrodes. When the pump volume (under constant pressure) and the e.m.f.

were steady to ± 0.01 cm^3 and ±1 mV, respectively, the system was considered to be at equilibrium. The time required to achieve this varied with the temperature and pressure. At high temperatures and low pressures, the system could reach equilibrium less than 4 h, while at high pressures more than 10 hours were required to satisfy the equilibrium criteria. At the end of each group of *p*H measurements, several state points were repeated to verify the repeatability of the experiments.

2.3 Chemical Samples

The source and purity of the chemical used are detailed in Table 3.

Table 3 Source and purity of the chemical samples, where x denoted mole-fraction purity, w denotes mass-fraction purity and ρ_e denotes electrical resistivity at $T = 298.15$ K [a].

Material	CAS Number	Purity as Supplied [a]	Source	Additional purification
Carbon dioxide	124-38-9	$x \geq 0.99995$	BOC	None
Nitrogen	7727-37-9	$x \geq 0.995$	BOC	None
Deionized water	7732-18-5	ρ_e >18 MΩ·cm	Millipore apparatus	Vacuum degassed
KCl	7447-40-7	$w \geq 0.99$	Sigma Aldrich	Oven dried
$KHCO_3$	298-14-6	$w \geq 0.997$	Sigma Aldrich	Oven dried
K_2CO_3	584-08-7	$w \geq 0.99$	Sigma Aldrich	Oven dried
0.01 M HCl (aq)	7674-01-0	$w \geq 0.9998$	Chem Lab-NV	None

[a] Mole- and mass-fraction purities are as stated by the supplier.

2.4 Calibration

The electrode system required calibration at every temperature and ionic strength to be studied. As established in previous work, the effect of pressure on the electrode calibration is negligible (Peng et al., 2013); therefore, the electrodes were calibrated with the reference solutions maintained under N_2 at pressure $p \leq 1.5$ MPa. Two reference solutions with *p*H of approximately 2 and 9 were used. The low *p*H reference contained 0.01 $mol \cdot kg^{-1}$ HCl, while the high *p*H reference was a buffer solution containing 0.0025 $mol \cdot kg^{-1}$ K_2CO_3 + 0.0025 $mol \cdot kg^{-1}$ $KHCO_3$. Both solutions were made up to the desired ionic strength by addition of KCl. The *p*H value of the reference solutions at given temperature was calculated, with the aid of the PHREEQC version 3.5.0 geochemical simulator, from the Pitzer model with the MacInnes convention. The Pitzer ion-interaction parameters were taken from Truche et al. (Truche et al., 2016), Plummer et al. (Plummer et al., 1988) and Appelo et al. (Appelo, 2015). These parameters and other necessary input data are listed in the Supplementary Information, together

with a sample input file for PHREEQC.

Table 4 Calibration data for the glass *p*H and Ag/AgCl reference electrodes at ionic strengths *I* and temperatures *T*, where *E* denotes e.m.f. at the specified *p*H. [a]

	T = 298.15 K		*T* = 308.15 K		*T* = 323.15 K		*T* = 343.15 K	
I	*p*H	*E*	*p*H	*E*	*p*H	*E*	*p*H	*E*
(mol·kg^{-1})	(-)	(mV)	(-)	(mV)	(-)	(mV)	(-)	(mV)
0.01	2.042	145.2	2.043	154.8	2.045	166.6	2.047	184.9
	10.153	-310.5	10.041	-308.6	9.885	-309.1	9.683	-303.7
1.08	2.079	163.7	2.088	173.4	2.102	186.9	2.122	208.8
	9.603	-277.4	9.510	-276.7	9.370	-277.1	9.214	-274.5
2.00	1.997	168.2	2.009	178.6	2.029	194.1	2.057	215.1
	9.495	-271.1	9.397	-269.7	9.273	-270.0	9.131	-266.5
4.00	1.805	183.3	1.823	194.2	1.851	208.2	1.889	229.4
	9.408	-263.2	9.317	-262.6	9.208	-262.0	9.088	-259.1

[a] Expanded uncertainties at 95% confidence are $U(T) = 0.05$ K and $U(E) = 2$ mV.

During the calibration process, a stable e.m.f was achieved with drift of less than 1 mV (equivalent to approximately 0.02 *p*H units) over 24 hours. The calibration data are given in Tables 4 for the glass electrode and Table 5 for the ZrO_2 electrode (small corrections were applied to the measured e.m.f. data to allow for small differences between the actual experimental temperature and the nominal temperatures listed). A linear relationship between the e.m.f. *E* and the solution *p*H was verified for these electrode systems in our previous work (Li et al., 2018) and therefore a two-point calibration with linear interpolation is justified.

Table 5 Calibration data for the ZrO_2 *p*H and Ag/AgCl reference electrodes at ionic strengths *I* and temperatures *T*, where *E* denotes e.m.f. at the specified *p*H. [a]

	T = 363.15 K		*T* = 393.15 K		*T* = 423.15 K	
I	*p*H	*E*	*p*H	*E*	*p*H	*E*
(mol·kg^{-1})	(-)	(mV)	(-)	(mV)	(-)	(mV)
2.00	2.087	784.3	2.137	797.1	2.194	797.7
	8.995	291.7	8.789	286.0	8.581	282.7
4.00	1.929	798.6	1.995	805.5	2.068	804.2
	8.975	349.6	8.792	336.5	8.602	322.3

[a] Expanded uncertainties at 95% confidence are $U(T) = 0.05$ K and $U(E) = 2$ mV.

2.5 Uncertainty

The overall combined standard uncertainty u_c of the *p*H measurements was calculated as follows:

$$u_c^2 = u_{pH}^2 + \left[\frac{\partial pH}{\partial T}u_T\right]^2 + \left[\frac{\partial pH}{\partial p}u_p\right]^2 + \left[\frac{\partial pH}{\partial E}u_E\right]^2 + \left[\frac{\partial pH}{\partial I}u_I\right]^2. \quad (1)$$

Here, u_T = 0.025 K is the standard uncertainty of temperature, u_p = 0.0325 MPa is the standard uncertainty of the pressure, u_E = 1 mV is the standard uncertainty of the e.m.f., u_I = 0.005 mol·kg^{-1} is the standard uncertainty of the ionic strength, and u_{pH} = 0.09 is the standard repeatability uncertainty. The overall uncertainty, dominated by the repeatability, is 0.1 for all state points investigated. Therefore, the expanded uncertainty at 95% confidence is 0.2.

3. Results and discussions

3.1 Validation measurements

Prior to starting the measurement on CO_2-saturated KCl solutions, verification experiments were carried out on CO_2-saturated water at T = 323.15 K and pressures up to 13.5 MPa. The results are shown in Fig. 2 in comparison with the experimental data of Peng et al. (Peng et al., 2013) and the predictions of the Pitzer model as implemented in PHREEQC. This good agreement serves to validate the two-point calibration strategy adopted in this work in comparison with the three-point calibration used by Peng et al.

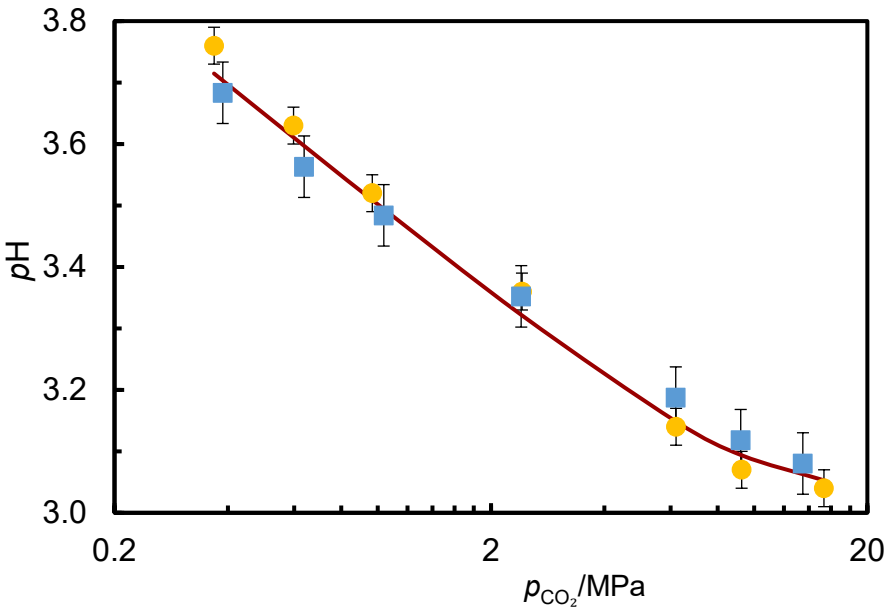

Fig. 2 *p*H of CO_2-saturated water as a function of CO_2 partial pressure at T = 323.15 K: ■, this work; ●, Peng et al. (Peng et al., 2013). The continuous line shows values calculated from the

PHREEQC software based on the Pitzer model. Error bar shows the combined standard uncertainty of the experimental data: $u(p\mathrm{H})$=0.03 for Peng et al. (Peng et al., 2013), and $u(p\mathrm{H})$ = 0.05 for this work.

3.2 The pH of CO_2-Saturated Aqueous KCl Solutions

The *p*H of CO_2-saturated aqueous KCl solution of ionic strengths 2 mol·kg^{-1} and 4 mol·kg^{-1} was measured at temperatures from 298.15 K to 423.15 K and at total pressures of between 0.2 MPa and 13.5 MPa. The temperatures and ionic strengths used correspond to values at which the electrode system had been calibrated and the *p*H was evaluated by linear interpolation using the appropriate entries in Tables 4 and 5. The glass electrode was used at the four lower temperatures studied and the ZrO_2 electrode was used for the three higher temperatures. The results are reported in Table 6. Measurements were repeated for the 2 mol·kg^{-1} brine at temperatures of (343.15 and 393.15) K and for the 4 mol·kg^{-1} brine at T = 308.15 K. All repeated measurements agreed with the tabulated data to with ±0.12 pH units and are compatible with the standard repeatability uncertainty of 0.09 *p*H units specified in section 2.5.

Table 6 Experimental *p*H of CO_2-saturated KCl (aq) at total pressure p, temperature T and salt molality m, where E is the measured e.m.f.[a]

p (MPa)	T (K)	E (mV)	*p*H (-)	p (MPa)	T (K)	E (mV)	*p*H (-)
m = 2 mol·kg^{-1}				m = 4 mol·kg^{-1}			
0.22	298.15	71.8	3.64	0.21	298.15	76.4	3.63
0.23	308.15	82.6	3.59	0.20	308.15	95.5	3.44
0.23	323.15	86.9	3.70	0.21	323.15	103.4	3.49
0.23	343.15	86.2	3.95	0.21	343.15	104.8	3.73
0.26	363.15	653.2	3.92	0.26	363.15	655.5	4.17
0.27	393.15	626.2	4.36	0.27	393.15	633.2	4.49
0.51	298.15	80.2	3.50	0.50	298.15	93.7	3.33
0.51	308.15	87.8	3.51	0.50	308.15	104.4	3.30
0.51	323.15	89.6	3.66	0.50	323.15	109.7	3.39
0.51	343.15	97.0	3.79	0.50	343.15	117.5	3.54
0.55	363.15	673.2	3.65	0.56	363.15	666.8	4.00
0.56	393.15	654.3	3.99	0.55	393.15	658.5	4.13
0.56	423.15	612.2	4.49	0.55	423.15	605.0	4.77
0.90	298.15	89.4	3.34	0.90	298.15	102.3	3.19
0.91	308.15	95.8	3.37	0.90	308.15	108.0	3.24

p (MPa)	T (K)	E (mV)	pH (-)	p (MPa)	T (K)	E (mV)	pH (-)
m = 2 mol·kg^{-1}				m = 4 mol·kg^{-1}			
0.90	323.15	93.5	3.60	0.90	323.15	114.4	3.32
0.93	363.15	675.3	3.62	0.90	343.15	118.9	3.52
0.92	393.15	663.7	3.87	0.91	363.15	683.7	3.73
0.92	423.15	639.9	4.15	0.93	393.15	667.6	3.99
2.00	298.15	93.9	3.27	0.92	423.15	643.5	4.25
2.00	308.15	100.7	3.29	2.00	298.15	110.4	3.05
2.00	323.15	106.8	3.39	2.00	308.15	118.3	3.07
2.00	343.15	112.3	3.57	2.00	323.15	123.3	3.18
2.02	363.15	687.5	3.44	2.00	343.15	133.2	3.31
2.00	393.15	673.9	3.74	2.04	363.15	698.0	3.51
2.01	423.15	656.0	3.95	2.04	393.15	686.3	3.72
4.31	298.15	102.1	3.12	2.04	423.15	670.7	3.88
4.31	308.15	109.8	3.14	4.30	298.15	119.9	2.89
4.31	323.15	115.3	3.26	4.31	308.15	130.3	2.87
4.32	343.15	121.3	3.43	4.31	323.15	137.8	2.95
4.30	363.15	701.8	3.24	4.30	343.15	145.2	3.13
4.30	393.15	688.0	3.56	4.32	363.15	711.2	3.30
4.30	423.15	672.7	3.74	4.34	393.15	698.4	3.55
9.26	298.15	103.9	3.09	4.32	423.15	685.4	3.68
9.26	308.15	116.2	3.04	9.25	298.15	125.3	2.79
9.26	323.15	125.4	3.10	9.25	308.15	138.0	2.74
9.26	343.15	133.1	3.26	9.25	323.15	147.4	2.80
9.27	363.15	710.2	3.13	9.25	343.15	156.6	2.96
9.26	393.15	701.8	3.38	9.26	363.15	724.1	3.10
9.26	423.15	690.1	3.53	9.25	393.15	711.8	3.35
13.54	298.15	105.0	3.08	9.26	423.15	699.6	3.49
13.55	308.15	117.1	3.02	13.50	298.15	118.4	2.91
13.51	323.15	127.3	3.07	13.50	308.15	136.3	2.77
13.52	343.15	136.7	3.21	13.50	323.15	147.6	2.80
13.56	363.15	711.1	3.11	13.50	343.15	157.7	2.95
13.57	393.15	704.5	3.34	13.56	363.15	727.5	3.04
13.56	423.15	694.2	3.48	13.55	393.15	715.8	3.30
				13.55	423.15	706.6	3.39

[a] Expanded uncertainties at 95% confidence are $U(p)$ = 0.065 MPa, $U(T)$ = 0.05 K, $U(E)$ = 2 mV and $U(p\text{H})$ = 0.20.

The experimental data are plotted along isotherms in Fig. 3 as a functions of the CO_2 partial pressure p_{CO_2}. The partial pressures were obtained by subtracting the vapor pressure of water p_{H_2O} from the measured total pressure, where p_{H_2O} was calculated from the equation of state of Wagner and Pruess (Wagner and Pruß, 2002). This is an approximation because the presence of salt slightly lowers the partial pressure of water; however, the effect of this approximation is not material on the scale of Fig. 3. Fig. 4 shows the same data plotted along lines of constant CO_2 partial pressure as functions of temperature; here, linear interpolation was used to align the data to nominal values of p_{CO_2}. Also shown in Fig. 3 and Fig. 4 (as continuous curves) are the corresponding *p*H values calculated from the Pitzer model implemented in PHREEQC version 3.5.0. Again, calculated *p*H values are based on the MacInnes convention (MacInnes, 1919) and the Pitzer ion-interaction parameters reported by Truche et al. (Truche et al., 2016), Plummer et al. (Plummer et al., 1988) and Appelo et al. (Appelo, 2015).

It can be observed that the experimental results span an interval from *p*H 2.7 to *p*H 4.8 over the temperatures and pressures ranges studied. In general, the *p*H decreases with increasing partial pressure and increases with increasing temperature. Moreover, a linear relationship between the *p*H $\ln(p_{CO_2})$ is observed at constant temperature and salinity up to partial pressures of between 2 MPa and 5 MPa, depending upon temperature. At higher partial pressures of CO_2, the *p*H gradually levels off to a plateau. Similar trends have been reported in the literature (Haghi et al., 2017; Li et al., 2018; Meyssami et al., 1992; Peng et al., 2013; Rosenqvist et al., 2012; Truche et al., 2016). This is attributed mainly to the solubility behavior of CO_2 in water or brine, which increases linearly with pressure at low pressures but more slowly at higher pressures where the product of partial molar volume and pressure becomes appreciable in comparison with RT (R is the universal gas constant).

On the other hand, the effect of temperature is more limited, with the *p*H increasing by approximately 0.5 units across the experimental temperature range. This is also consistent with the trend observed in the literature for similar systems (Shao et al., 2013; Truche et al., 2016). We also note that the slope with respect to temperature declines at low temperatures and high pressures leading to the isobars converging.

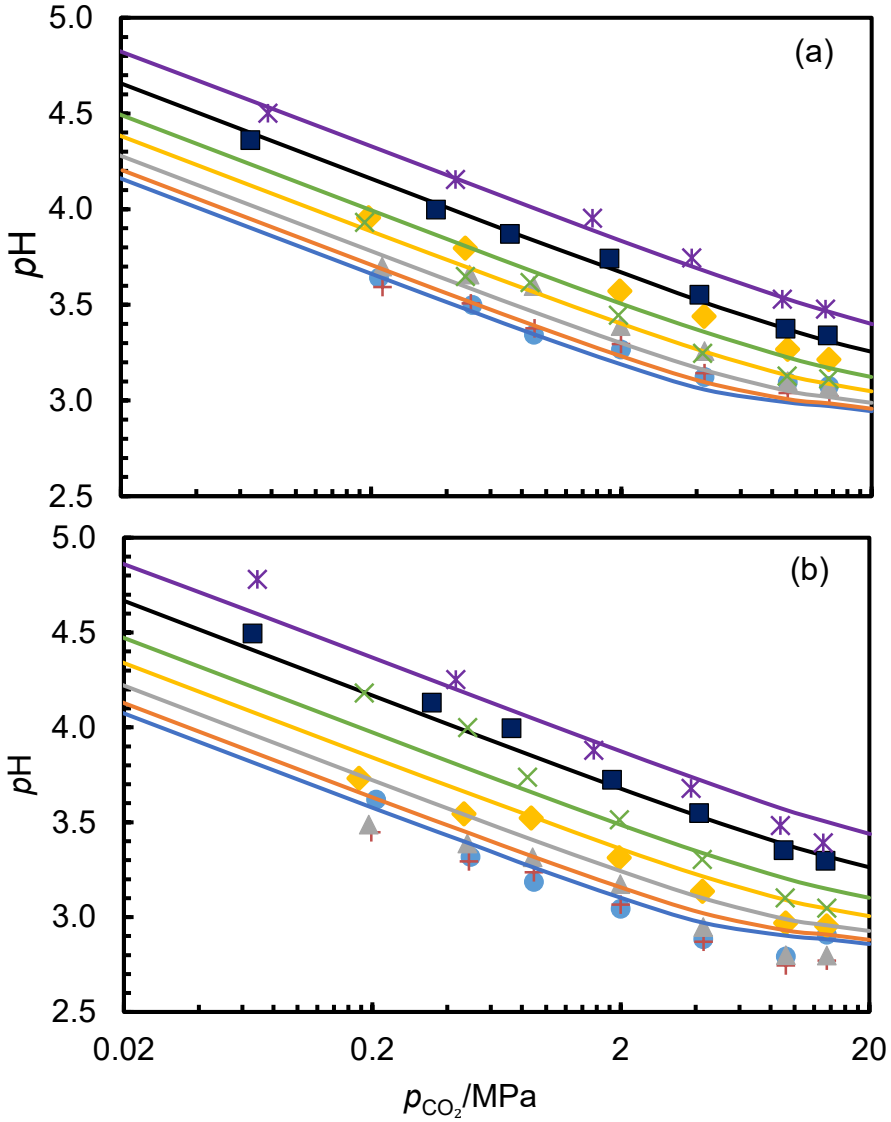

Fig. 3 *p*H of CO_2-saturated KCl (aq) as a function of CO_2 partial pressure (a) m = 2.0 mol·kg^{-1} and (b) m = 4.0 mol·kg^{-1}: ●, T = 298.15 K ; +, T = 308.15 K;▲, T = 323.15 K; ◆, T = 343.15 K;×, T = 363.15 K; ■, T = 393.15 K; ∗, T = 423.15 K. Continuous lines are calculated from the Pitzer model using the PHREEQC 3.5.0 software.

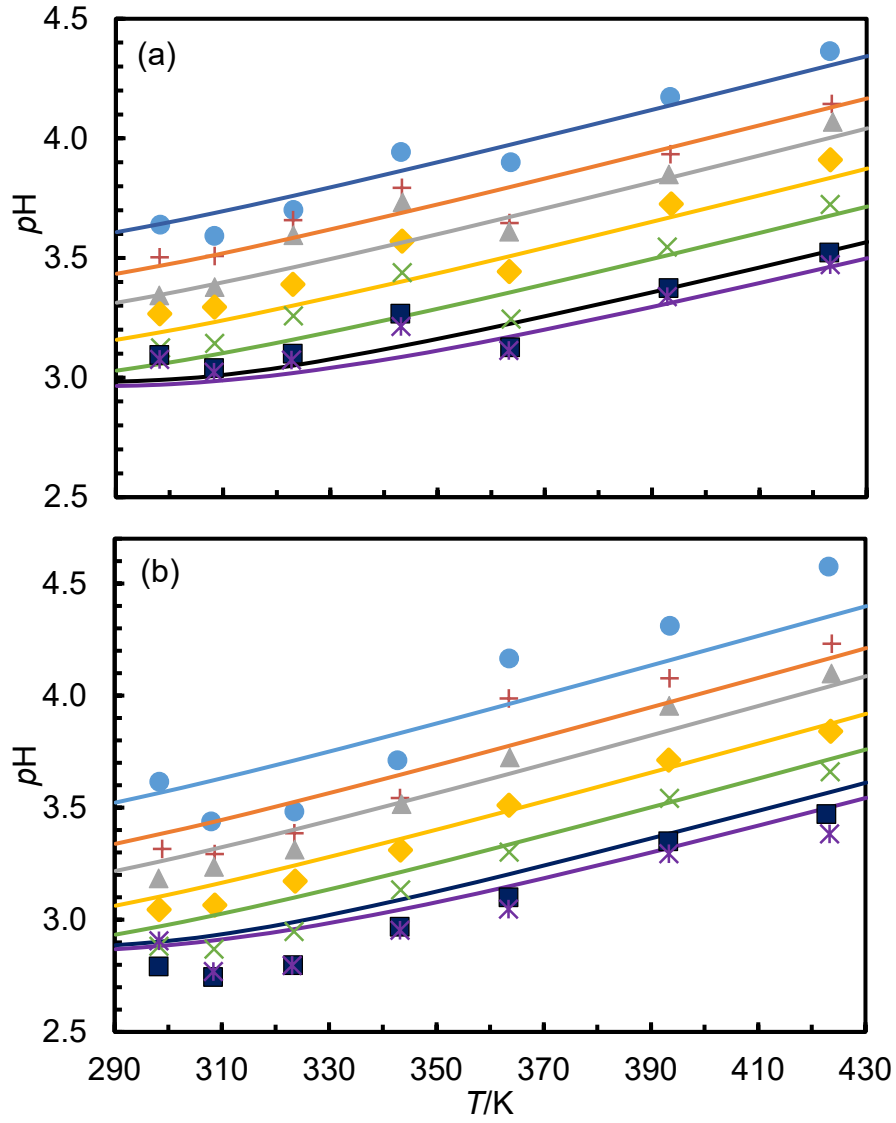

Fig. 4 *p*H of CO_2-saturated KCl (aq) as a function of CO_2 partial pressure (a) m = 2.0 mol·kg^{-1} and (b) m = 4.0 mol·kg^{-1}: ●, p_{CO_2} = 0.22 MPa; +, p_{CO_2} = 0.50 MPa; ▲, p_{CO_2} = 0.90 MPa; ◆, p_{CO_2} = 2.0 MPa; ×, p_{CO_2} = 4.3 MPa; ■, p_{CO_2} = 9.3 MPa; ∗, p_{CO_2} = 13.5 MPa. Continuous lines are calculated from the Pitzer model using the PHREEQC 3.5.0 software.

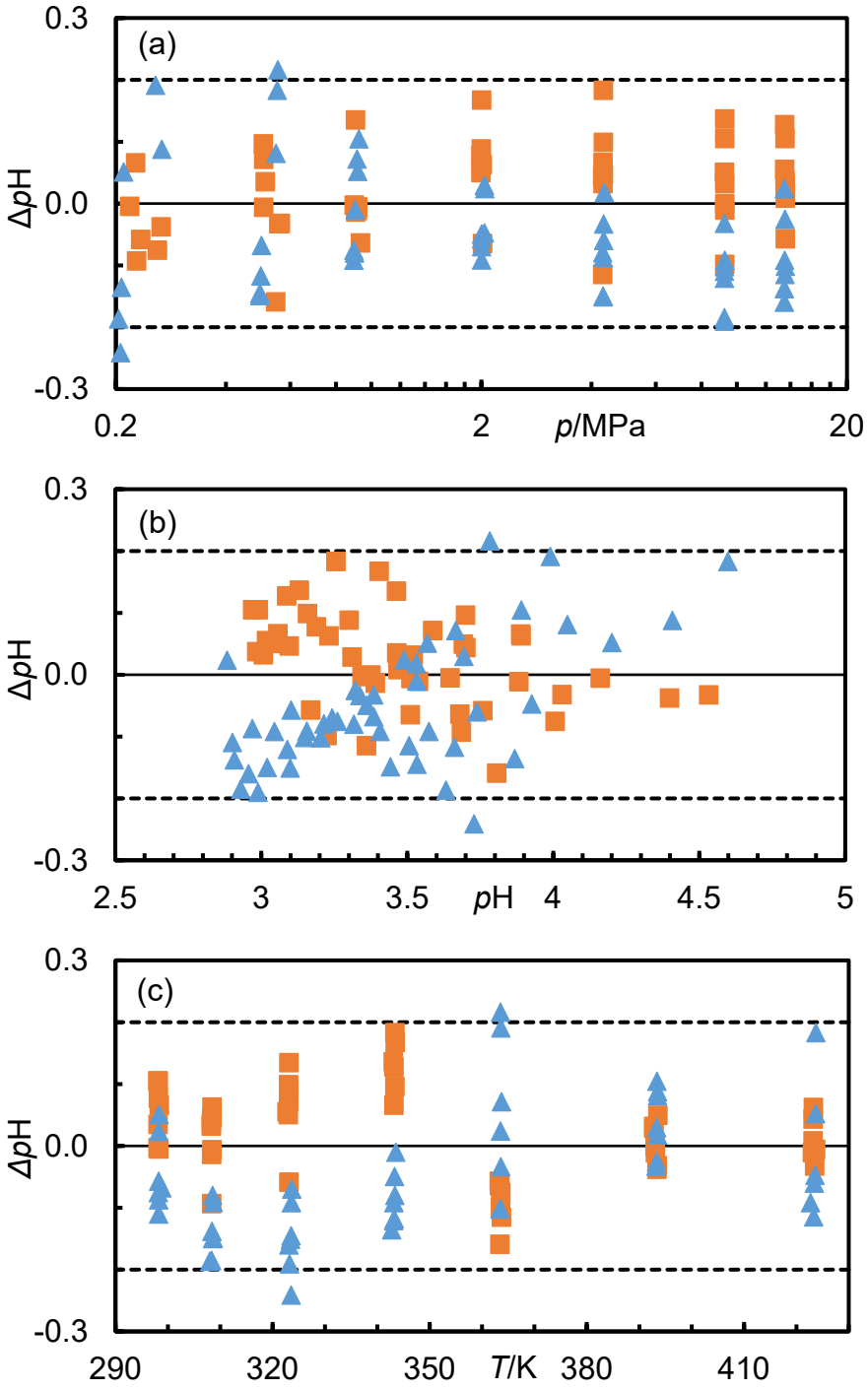

Fig. 5 Deviation Δ*p*H = *p*H(experimental) – *p*H(calculated) of the measured *p*H from values calculated from the Pitzer model for CO_2-saturated KCl (aq) as a function of (a) pressure *p*, (b) *p*H and (c) temperature *T* for ionic strengths:■, $m = 2.0$ mol·kg^{-1}; ▲, $m = 4.0$ mol·kg^{-1}. Dashed lines represent the 95% confidence interval for the experimental data.

Comparison with the predictions of the Pitzer model indicate generally good agreement. This is shown in more detail in Fig. 5 where we plot deviations of the experimental data from the Pitzer model as functions of pressure, *p*H and temperature. Almost all the measured data fall within the 95% conference interval based on the experimental uncertainty and the deviations are quite similar in magnitude at both salinities investigated.

Concerning the influence of salinity, it is observed in this work that the *p*H of CO_2 saturated KCl solutions decreases with increase in salt molality when temperature and pressure are constant. This trend has also been reported for CO_2 saturated NaCl solutions (Haghi et al., 2017; Li et al., 2018; Truche et al., 2016), although Schaef (Schaef et al., 2003) observed the inverse behavior. Haghi et al. (Haghi et al., 2017) suggest that reported increases of *p*H with salinity are erroneous and caused by diffusion of NaCl into the liquid junction of the *p*H probes. In the present work, we observed stable *p*H readings over time suggesting that diffusion was not a problem.

Another view on the experimental data is afforded by plotting *p*H against $px = -\log_{10}(x)$, where x is the mole fraction of CO_2 in the solution. In previous work, this has been found to exhibit linear behavior (Li et al., 2018; Peng et al., 2013) (Truche et al., 2016). To study this relationship for the present system, we used a solubility model to estimate the mole fraction of dissolved CO_2. However, common solubility models such as those of Duan et al. (Duan et al., 2006) and Spycher and Pruss (Spycher and Pruess, 2010) treat the influence of K^+ as being the same as that of Na^+, which is demonstrably not the case (Hou et al., 2013). To address this problem, we developed a modification to the Spycher and Pruss model (Spycher and Pruess, 2010) to treat K^+ ions explicitly. In this approach, the salting-out effect is modelled by a factor γ'_{CO_2} in the CO_2 activity coefficient which may be written as follows:

$$\gamma'_{CO_2} = \left(1 + M_w \sum_{i \neq CO_2} m_i\right) \exp\left[2\lambda\left(m_{Na} + \chi m_K + 2m_{Ca} + 2m_{Mg}\right) + \xi m_{Cl}\left(m_{Na} + m_K + m_{Ca} + m_{Mg}\right) - 0.07 m_{SO_4}\right]. \quad (2)$$

Here, $M_w = 0.018015$ kg·mol^{-1} is the molar mass of water, m_i is the molality of the i^{th} aqueous species and λ and ξ are temperature dependent interaction parameters given by Spycher and Pruss (Spycher and Pruess, 2010). In the original model, the parameter χ was unity (so that K^+ and Na^+ were equivalent) but this condition was relaxed in the present work. To determine χ as a function of temperature, we regressed the solubility data reported by Hou et al (Hou et al., 2013) for CO_2 in aqueous KCl solutions. The results are shown in Fig 6 where the CO_2 solubility is expressed as a molality and the KCl molalities were 2.5 and 4.0 mol·kg^{-1}. It can

be seen that the original model fails to follow the experimental data, whereas our new model provides a much better fit. In this analysis we made χ a linear function of temperature and the optimal fit was obtained with

$$\chi = 0.122 + 0.00202(T / \mathrm{K}) . \tag{3}$$

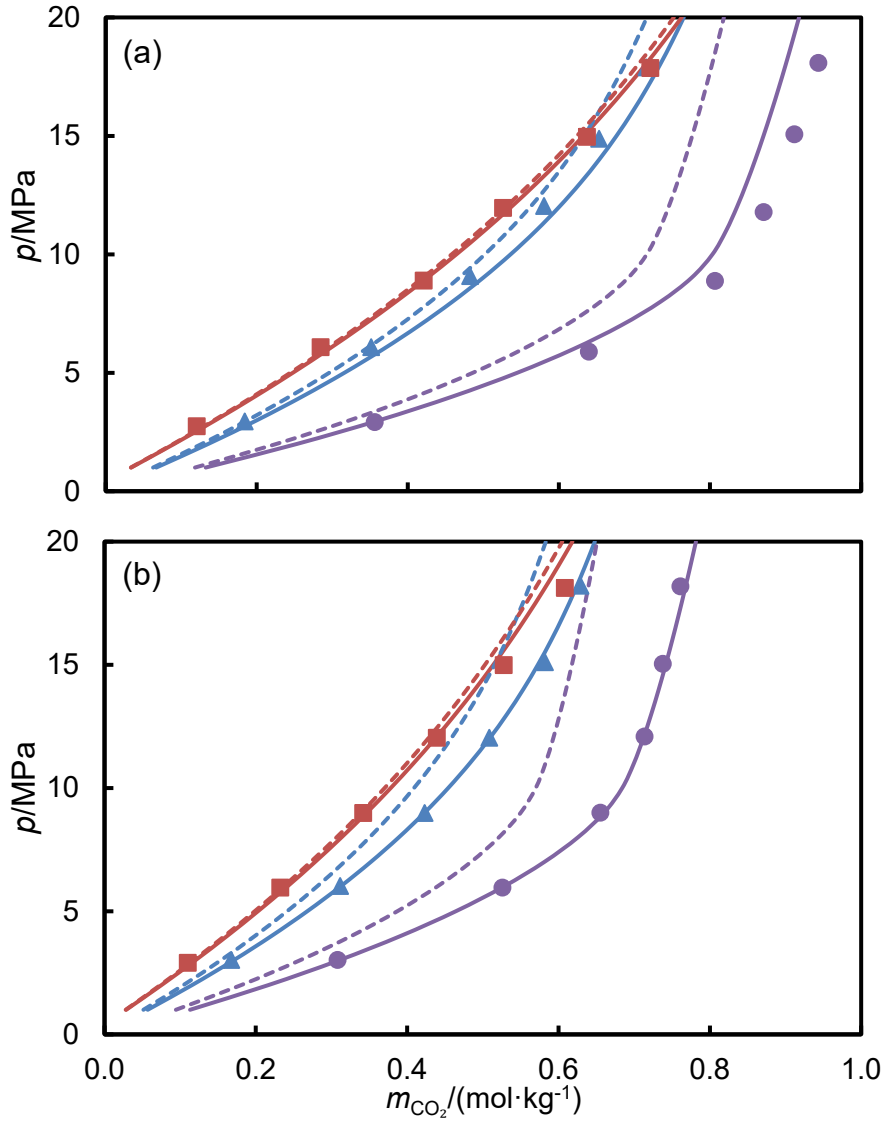

Fig. 6 Comparison between predicted and experimental (Hou et al., 2013) molality of CO_2 dissolved in aqueous KCl solutions of different molalities: (a) 2.5 mol·kg^{-1}; (b) 4.0 mol·kg^{-1}. Symbols: ●, T =323.15 K; ▲, T = 373.15 K; ■, T =423.15 K. Dashed lines and continues lines represent the prediction based on the original and modified Spycher and Pruess model (Spycher and Pruess, 2010), respectively.

To quantify the goodness of fit, we calculate the average absolute deviations between the experimental data and the model. For a property X, this is defined as follows

$$\Delta_{\mathrm{AAD}}(X) = N^{-1}\sum_{i=1}^{N}\left|X_{i,\mathrm{exp}} - X_{i,\mathrm{calc}}\right|, \tag{4}$$

where $X_{i,\mathrm{exp}}$ is the i^{th} experimental datum, $X_{i,\mathrm{calc}}$ is the value calculated from the model at the same state point and N is the number of data points. For the CO_2-solubility data, state points are defined by temperature, pressure and salt molality and we find $\Delta_{\mathrm{AAD}}(m_{CO_2}) = 0.012$ mol·kg^{-1} for the whole data set. The mole fraction of dissolved CO_2, calculated in a salt-free basis, is then given by $x = m_{CO_2}/(m_{CO_2} + M_w^{-1})$, where M_w is the molar mass of water.

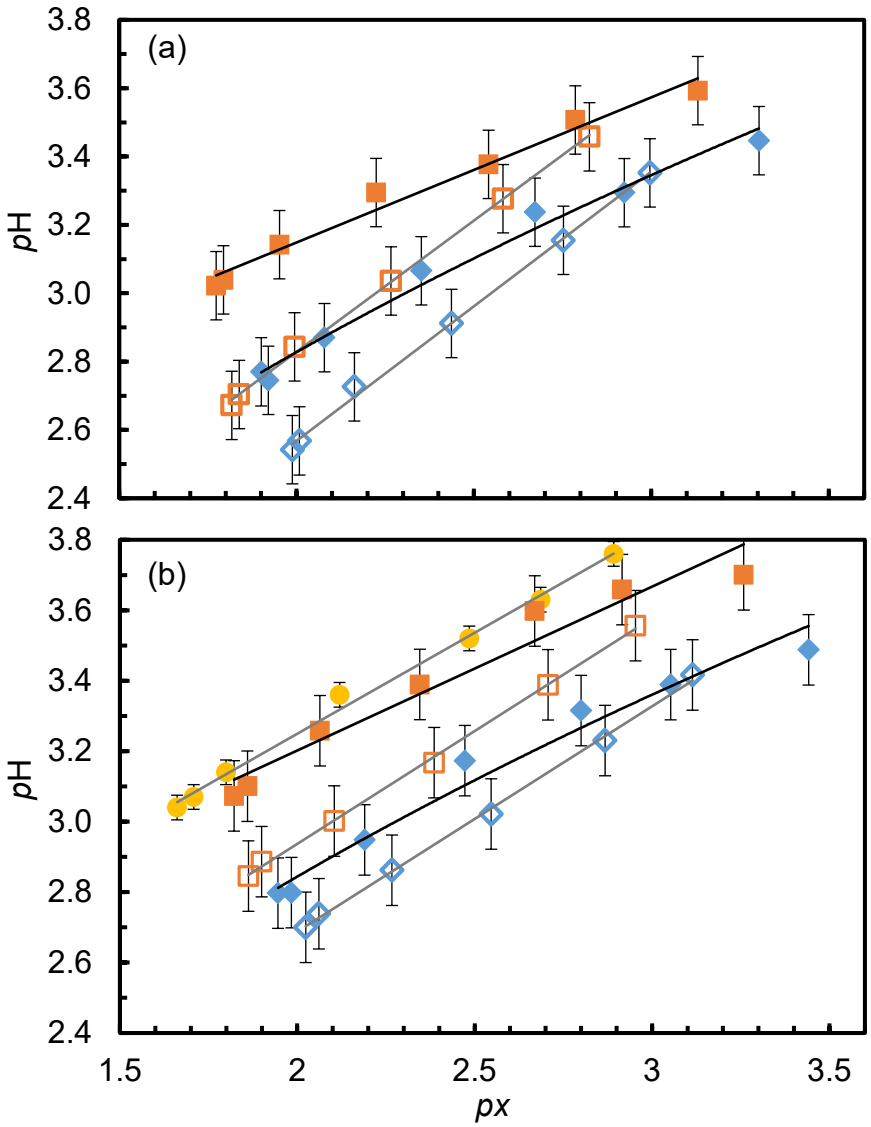

Fig. 7 *p*H of CO_2-saturated KCl (aq) (this work), NaCl (aq) (Li et al., 2018) and water (Peng et al., 2013) as functions of $px = -\log_{10}(x)$, where x is the calculated mole fraction of CO_2 in the aqueous solution, at (a) $T = 308.15$ K and (b) $T = 323.15$ K. Symbols: ●, pure water; ■, KCl (aq) $m = 2.0$ mol·kg^{-1}; ◆, KCl (aq) $m = 4.0$ mol·kg^{-1}; □, NaCl (aq) $m = 2$ mol·kg^{-1}; ◇, NaCl (aq) $m = 4$ mol·kg^{-1}. Lines represent Eq. (5) with best-fit parameters.

The relation between *p*H and *px* is illustrated at temperatures of 308.15 K and 323.15 K in Fig. 7. Here we show the results for CO_2 in the aqueous KCl solutions investigated in this work and for CO_2 in pure water and in NaCl solutions from the literature (Li et al., 2018; Peng et al., 2013). In (Li et al., 2018), measurements were reported for CO_2 in NaCl (aq) at molalities of (1, 3 and 5) mol·kg^{-1} and, to facilitate the comparison, these were interpolated to NaCl molalities of (2 and 4) mol·kg^{-1}. Each of the systems depicted in Fig. 7 shows a superficially-linear relation between *p*H and *px*, which we express as：

$$pH = A(px) + B\,. \tag{5}$$

A similar linear correlation was observed by Truche et al. at temperatures between 473 K and 553 K for CO_2 in both water and 1.4 mol·kg^{-1} NaCl (aq) (Truche et al., 2016). The coefficients *A* and *B*, their respective standard uncertainties *u*(*A*) and *u*(*B*), and the average absolute deviation of *p*H determined from the present results in KCl brines are given in Table 7.

Table 7. Parameters *A* and *B*, and their respective standard uncertainties *u*(*A*) and *u*(*B*), in the linear correlation of *p*H against *px* for CO_2-saturated KCl brines of molality *m*.

T (K)	*A*	*u*(*A*)	*B*	*u*(*B*)	AAD	*A*	*u*(*A*)	*B*	*u*(*B*)	AAD
	m = 2 mol·kg^{-1}					*m* = 4 mol·kg^{-1}				
298.15	0.428	0.018	2.336	0.041	0.01	0.563	0.043	1.776	0.105	0.03
308.15	0.424	0.027	2.300	0.064	0.03	0.503	0.038	1.829	0.094	0.03
323.15	0.466	0.048	2.269	0.118	0.05	0.490	0.048	1.881	0.124	0.05
343.15	0.462	0.028	2.380	0.072	0.03	0.502	0.035	1.961	0.096	0.04
363.15	0.499	0.026	2.133	0.070	0.03	0.721	0.026	1.564	0.074	0.02
393.15	0.492	0.015	2.383	0.043	0.02	0.606	0.011	2.032	0.034	0.01
423.15	0.526	0.019	2.450	0.053	0.02	0.726	0.035	1.822	0.103	0.04

Fig. 8 compares the present values of *A* and *B* with those reported the literature for CO_2-saturated water and NaCl brines. Here we can see that the *B* parameter in Eq. (5) for KCl solutions is quite similar to that for water, whereas the same parameter for NaCl solution shows a much more pronounced dependence upon temperature. The slope parameter *A* for KCl solutions is mostly smaller than in pure water but it has a slight upward trend with temperature whereas, on the whole, the values for water exhibit a decreasing trend with increasing temperature. Again the data for NaCl solutions vary more rapidly with temperature.

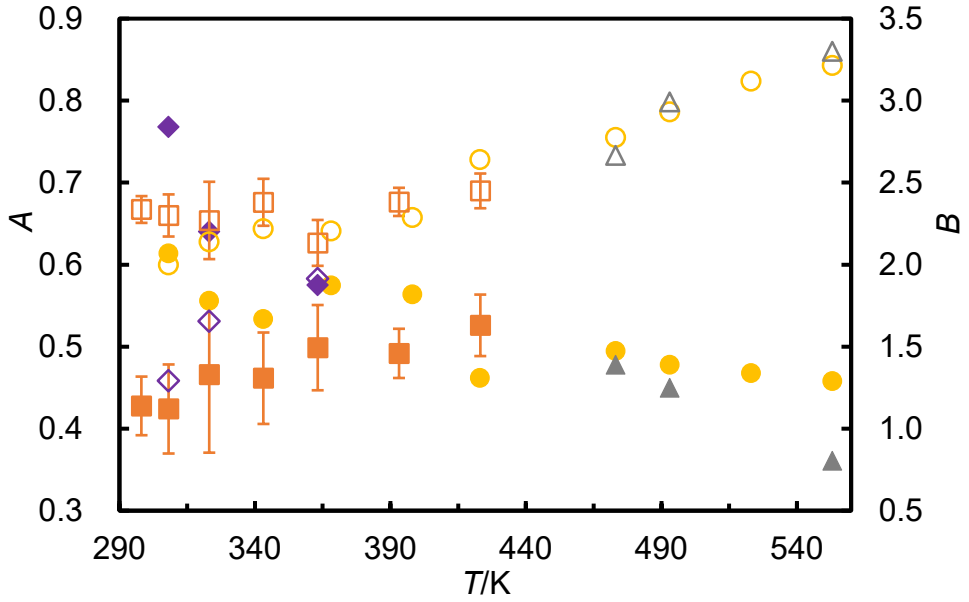

Fig 8 Parameters *A* (filled symbols) and *B* (open symbols) in the linear correlation between *p*H and *px* as functions of temperature for different brines: ●,○ water, Truche (Truche et al., 2016); ▲,△ NaCl (aq) $m = 1.4$ mol·kg^{-1}, Truche (Truche et al., 2016); ◆,◇ NaCl (aq) $m = 2.0$ mol·kg^{-1}, Li et al. (Li et al., 2018); ■,□ KCl (aq) $m = 2.0$ mol·kg^{-1} (this work); error bars show 95% confidence intervals (this work only).

4. Conclusions

In this paper, the *p*H of CO_2-saturated aqueous KCl solutions was measured over wide ranges of temperature and pressure and at salt molalities of 2 mol·kg^{-1} and 4 mol·kg^{-1}. The range of conditions investigated covers those relevant to CO_2 storage in deep saline aquifers. The key findings are that the influence of KCl on *p*H under conditions of constant temperature and CO_2 partial pressure is different from that of NaCl, with the *p*H in the former generally being slightly higher. This difference of behavior would probably only be significant in brines containing high molalities of K^+ and it would still be reasonable to treat Na+ and K+ as approximately equivalent at low K^+ molalities. The Pitzer model as implemented in PHREEQC version 3.5.0 was found to provide a generally good prediction of the experimental data and hence the present work serves to validate that model for the prediction of *p*H in systems involving CO_2 dissolved in KCl (aq).

Supporting information

Available Supporting Information: input parameters for PHREEQC 3.5.0 calculations based on the Pitzer model (Tables A.1-A.3).

Funding

This work was supported by an award from the China Scholarship Council and funding from XinJiang Autonomous Region Innovation Environment (talents, base) construction special project - youth fund for natural science.

Appendix A Supplementary material

Available Supporting Information: input parameters for PHREEQC 3.5.0 calculations based on the Pitzer model (Tables A.1–A.3). Supplementary data to this article can be found online at https://doi.org/10.1016/j.ces.2020.116434.

References

Aggelopoulos, C.A., Robin, M., Perfetti, E., Vizika, O., 2010. CO_2/$CaCl_2$ solution interfacial tensions under CO_2 geological storage conditions: Influence of cation valence on interfacial tension. Advances in Water Resources 33, 691-697.

Alkhaldi, M.H., Nasr-El-Din, H.A., Sarma, H.K., 2010. Kinetics of the reaction of citric acid with calcite. SPE Journal 15, 704-713.

Appelo, C.A.J., 2015. Principles, caveats and improvements in databases for calculating hydrogeochemical reactions in saline waters from 0 to 200 °C and 1 to 1000 atm. Applied Geochemistry 55, 62-71.

Bachu, S., 2000. Sequestration of CO_2 in geological media: criteria and approach for site selection in response to climate change. Energy Conversion and Management 41, 953-970.

Byrne, R.H., Breland, J.A., 1989. High precision multiwavelength pH determinations in seawater using cresol red. Deep Sea Research Part A. Oceanographic Research Papers 36, 803-810.

Clayton, T.D., Byrne, R.H., 1993. Spectrophotometric seawater pH measurements: total hydrogen ion concentration scale calibration of m-cresol purple and at-sea results. Deep Sea Research Part I: Oceanographic Research Papers 40, 2115-2129.

Covington, A., Bates, R., Durst, R., 1985. Definition of pH scales, standard reference values, measurement of pH and related terminology (Recommendations 1984). Pure and Applied Chemistry 57, 531-542.

Crolet, J., Bonis, M., 1983. pH measurements in aqueous CO_2 solutions under high pressure and temperature. Corrosion 39, 39-46.

Druckenmiller, M.L., Maroto-Valer, M.M., 2005. Carbon sequestration using brine of adjusted pH to

form mineral carbonates. Fuel Processing Technology 86, 1599-1614.

Duan, Z., Sun, R., Zhu, C., Chou, I.M., 2006. An improved model for the calculation of CO_2 solubility in aqueous solutions containing Na^+, K^+, Ca^{2+}, Mg^{2+}, Cl^-, and SO_4^{2-}. Marine Chemistry 98, 131-139.

Haghi, R.K., Chapoy, A., Peirera, L.M.C., Yang, J., Tohidi, B., 2017. pH of CO_2 saturated water and CO_2 saturated brines: Experimental measurements and modelling. International Journal of Greenhouse Gas Control 66, 190-203.

Hanor, J.S., 1994. Origin of saline fluids in sedimentary basins. Geological Society, London, Special Publications 78, 151.

Hinds, G., Cooling, P., Wain, A., Zhou, S., Turnbull, A., 2009. Technical Note: Measurement of pH in Concentrated Brines. Corrosion 65, 635-638.

Hoballah, R., 2017. On the Solubility of Acid and Sour Gases in Water and Brines Under Reservoir Conditions, Chemical Engineering (New York). Imperial College London.

Hou, S.-X., Maitland, G.C., Trusler, J.P.M., 2013. Phase equilibria of (CO_2 + H_2O + NaCl) and (CO_2 + H_2O + KCl): Measurements and modeling. The Journal of Supercritical Fluids 78, 78-88.

Hyde, A.M., Zultanski S.L., Waldman J.H., Zhong Y.L., Shevlin M., Peng F., 2017. General principles and strategies for salting-out informed by the Hofmeister series. Organic Process Research & Development 21, 1355–1370.

Kaszuba, J.P., Janecky, D.R., Snow, M.G., 2003. Carbon dioxide reaction processes in a model brine aquifer at 200 °C and 200 bars: implications for geologic sequestration of carbon. Applied Geochemistry 18, 1065-1080.

Kimuro, B., Kusayanagi, T., Yamaguchi, F., Ohtsubo, K., Morishita, M., 1994. Basic experimental results of liquid CO_2 injection into the deep ocean. IEEE transactions on energy conversion 9, 732-735.

Li, X., Peng, C., Crawshaw, J.P., Maitland, G.C., Trusler, J.P.M., 2018. The pH of CO_2-saturated aqueous NaCl and NaHCO3 solutions at temperatures between 308 K and 373 K at pressures up to 15 MPa. Fluid Phase Equilibria 458, 253-263.

MacInnes, D.A., 1919. The Activities of the Ions of Strong Electrolytes. Journal of the American Chemical Society 41, 1086-1092.

Marion, G.M., Millero, F.J., Camões, M.F., Spitzer, P., Feistel, R., Chen, C.T.A., 2011. pH of seawater. Marine Chemistry 126, 89-96.

Metz, B., O. Davidson, H. C. de Coninck, M. Loos, and L. A. Meyer, 2005. IPCC special report on carbon dioxide capture and storage. Cambridge University Press, Cambridge, United Kingdom and New York, NY, USA.

Meyssami, B., Balaban, M.O., Teixeira, A.A., 1992. Prediction of pH in Model Systems Pressurized with Carbon Dioxide. Biotechnology Progress 8, 149-154.

Millero, F.J., DiTrolio, B.R., Suarez, A.F., Lando, G., 2009. Spectroscopic measurements of the pH in NaCl brines. Geochimica et Cosmochimica Acta 73, 3109-3114.

Morse, J.W., Arvidson, R.S., 2002. The dissolution kinetics of major sedimentary carbonate minerals. Earth-Science Reviews 58, 51-84.

Parkhurst, D.L., Appelo, C.A.J., 2013. Description of input and examples for PHREEQC version 3: a computer program for speciation, batch-reaction, one-dimensional transport, and inverse geochemical calculations, U.S. Geological Survey Techniques and Methods, book 6, Denver, CO, U.S.A., p. 519.

Parton, T., Spilimbergo, S., Elvassore, N., Bertucco, A., 2002. UV–VIS spectroscopy for the determination of diffusion coefficient and pH in aqueous solutions/sc-CO_2 systems, 4th International Symposium on High Pressure Process Technology and Chemical Engineering, Venice, Italy, Lido di Venezia, Italy, pp. 447-452.

Peng, C., Crawshaw, J.P., Maitland, G.C., Trusler, J.P.M., Vega-Maza, D., 2013. The pH of CO_2-saturated water at temperatures between 308 K and 423 K at pressures up to 15 MPa. Journal of Supercritical Fluids 82, 129-137.

Pentland, C.H., El-Maghraby, R., Iglauer, S., Blunt, M.J., 2011. Measurements of the capillary trapping of super-critical carbon dioxide in Berea sandstone. Geophysical Research Letters 38, L06401.

Pitzer, K.S., 1973. Thermodynamics of Electrolytes . I. Theoretical Basis and General Equations. Journal of Physical Chemistry 77, 268-277.

Pitzer, K.S., 1975. Thermodynamics of Electrolytes .V. Effects of Higher-Order Electrostatic Terms. Journal of Solution Chemistry 4, 249-265.

Pitzer, K.S., 1991. Activity coefficients in electrolyte solutions. CRC Press, Boca Raton.

Pitzer, K.S., Mayorga, G., 1973. Thermodynamics of Electrolytes. II. Activity and Osmotic Coefficients for Strong Electrolytes with One or Both Ions Univalent. Journal of Physical Chemistry 77, 2300-2308.

Pitzer, K.S., Peiper, J.C., Busey, R.H., 1984. Thermodynamic Properties of Aqueous Sodium-Chloride Solutions. Journal of Physical and Chemical Reference Data 13, 1-102.

Plummer, L.N., Parkhurst, D.L., Fleming, G.W., Dunkle, S.A., 1988. A Computer Program Incorporating Pitzer's Equations for Calculation of Geochemical Reactions in Brines, Water-Resources Investigations Report.

Robert-Baldo, G.L., Morris, M.J., Byrne, R.H., 1985. Spectrophotometric determination of seawater pH using phenol red. Analytical Chemistry 57, 2564-2567.

Rosenqvist, J., Kilpatrick, A.D., Yardley, B.W.D., 2012. Solubility of carbon dioxide in aqueous fluids and mineral suspensions at 294K and subcritical pressures. Applied Geochemistry 27, 1610-1614.

Ruaya, J.R., Seward, T.M., 1987. The ion-pair constant and other thermodynamic properties of HCl up to 350°C. Geochimica et Cosmochimica Acta 51, 121-130.

Schaef, H.T., McGrail, B.P., Marti, P.F., 2003. Direct Measurements of pH and Dissolved CO_2 Concentrations in H_2O-CO_2-NaCl Mixtures to Supercritical Conditions, Carbon Sequestration Second Annual Conference, Alexandria, Virginia.

Schaef, T.H., McGrail, P.B., 2005. Direct measurements of pH and dissolved CO_2 in H_2O-CO_2 brine mixtures to supercritical conditions, Greenhouse Gas Control Technologies 7. Elsevier Science Ltd, Oxford, pp. 2169-2173.

Shao, H., Thompson, C.J., Cantrell, K.J., 2013. Evaluation of experimentally measured and model-calculated pH for rock–brine–CO_2 systems under geologic CO_2 sequestration conditions. Chemical Geology 359, 116-124.

Spycher, N., Pruess, K., 2010. A Phase-Partitioning Model for CO_2–Brine Mixtures at Elevated Temperatures and Pressures: Application to CO_2-Enhanced Geothermal Systems. Transport in Porous Media 82, 173-196.

Stefánsson, A., Bénézeth, P., Schott, J., 2013. Carbonic acid ionization and the stability of sodium bicarbonate and carbonate ion pairs to 200 °C – A potentiometric and spectrophotometric study. Geochimica et Cosmochimica Acta 120, 600-611.

Toews, K.L., Shroll, R.M., Wai, C.M., Smart, N.G., 1995. pH-Defining Equilibrium between Water and Supercritical CO_2. Influence on SFE of Organics and Metal Chelates. Analytical Chemistry 67, 4040-4043.

Truche, L., Bazarkina, E.F., Berger, G., Caumon, M.-C., Bessaque, G., Dubessy, J., 2016. Direct measurement of CO_2 solubility and pH in NaCl hydrothermal solutions by combining in-situ potentiometry and Raman spectroscopy up to 280° C and 150 bar. Geochimica et Cosmochimica Acta 177, 238-253.

Wagner, W., Pruß, A., 2002. The IAPWS formulation 1995 for the thermodynamic properties of ordinary water substance for general and scientific use. Journal of Physical and Chemical Reference Data 31, 387-535.

Wolery, T.J., 1983. EQ3NR: a computer program for geochemical aqueous speciation-solubility calculations User's guide and documentation, United States, p. 202.

Zhang, G.X., Zheng, Z.P., Wan, J.M., 2005. Modeling reactive geochemical transport of concentrated aqueous solutions. Water Resources Research 41.